

A complete computer aided engineering (CAE) modelling and optimization of high pressure die casting (HPDC) process

K. Dou^{*}, E. Lordan, Y.J. Zhang, A. Jacot, Z.Y. Fan

Brunel Centre for Advanced Solidification Technology (BCAST), Brunel University London, Kingston Lane, Uxbridge, UB8 3PH, United Kingdom

ARTICLE INFO

Keywords:

CAE simulation
finite element method
HPDC
Process optimization
CFD
Mechanical property

ABSTRACT

The application of computer aided engineering (CAE) has become a trend in manufacture industry due to its great efficiency and reliability. In casting industries, numerical modelling of the casting process based on CAE has replaced traditional trial-and-error R&D procedures in many aspects. With advanced parallel computing techniques and numerous calculation models, the fluid flow, heat transfer, solidification and defect formation behaviours under different casting conditions may be examined in detail. Based on this idea, component design and the optimization of casting parameters may be carried out to produce products for subsequent micro-structural and mechanical characterization. In this way, a direct link between process condition, casting quality, and cast mechanical properties may be established in a manner that is practical, economical and energy efficient for such processes as gravity die casting, high pressure die casting (HPDC) and continuous casting.

In this work, the entire HPDC process, including die heating, thermal die cycling, shot sleeve pre-filling, slow shot/fast shot injection, die filling/solidification as well as intensification, is simulated for an Al-Si alloy using the casting simulation package ProCAST. The interfacial heat transfer coefficients between melt and die wall/shot sleeve are adjusted according to thermal couple measurements and infrared imaging of the die surface temperature distribution. Based on this complete numerical model, the HPDC process may be optimized using the following methodology: 1) the optimum thermal die cycle number is determined after which the dynamic steady state of die temperature is obtained to guarantee relatively sound casting quality. 2) The piston shot profile is adjusted to reduce defect formation during injection. In the meantime, tensile bars are cast using the optimized piston shot profile and the mechanical properties (yield strength, ultimate tensile strength and elongation) are tested to assess the effectiveness of the computer simulation. Results show that the mechanical properties are improved with the optimized process parameters, providing further evidence that CAE could help in the optimization of HPDC processes.

Introduction

The application of the high pressure die casting (HPDC) process has enabled mass production of cast alloy components with high dimensional accuracy and great efficiency. Due to the inherently turbulent melt flow during injection, defects such as entrapped air, porosity and non-uniform grains are common and randomly distributed in HPDC components, which in turn deteriorate the mechanical properties. The design and layout of cast systems (gate and runner, overflows, vents) as well as the suitable configuration of casting parameters are vital factors influencing the melt flow characteristics during HPDC die filling. Proper configuration of gate and runner systems plus optimum casting parameters could lead to cast components with improved mechanical

properties and casting consistency. Zhou [1] designed a new runner which contained a collector for externally solidified crystals (ESCs) forming in shot sleeve and found that the mechanical properties of the cast alloys produced with the optimized runner system increased obviously. Gunasegaram [2] succeeded in achieving improved ultimate tensile strength (UTS) and elongation for HPDC aluminium alloys through optimization of runner design and increasing of piston velocity. Tsoukalas [3] investigated the influence of die casting machine parameters (piston velocity, intensification pressure, die cavity filling time) on formation of porosity in cast components and found that using optimal die casting machine parameter levels leads the optimum porosity value in final castings. Wu [4] observed the microstructure formation of magnesium alloy die castings produced with different

^{*} Corresponding author.

E-mail address: Kun.Dou@hotmail.com (K. Dou).

<https://doi.org/10.1016/j.jmapro.2020.10.062>

Received 22 October 2019; Received in revised form 21 October 2020; Accepted 21 October 2020

Available online 3 November 2020

1526-6125/© 2020 The Society of Manufacturing Engineers. Published by Elsevier Ltd. All rights reserved.

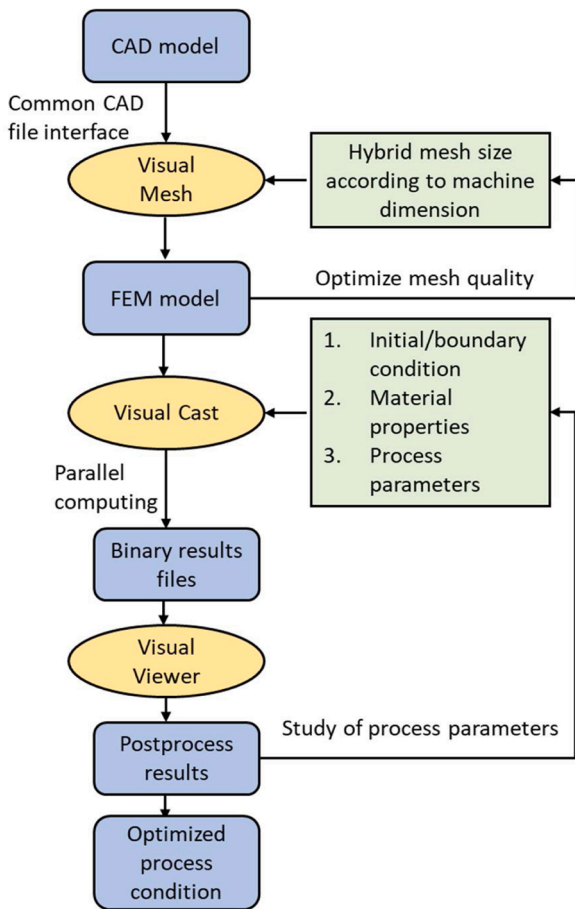


Fig. 1. Modelling workflow of the entire HPDC process.

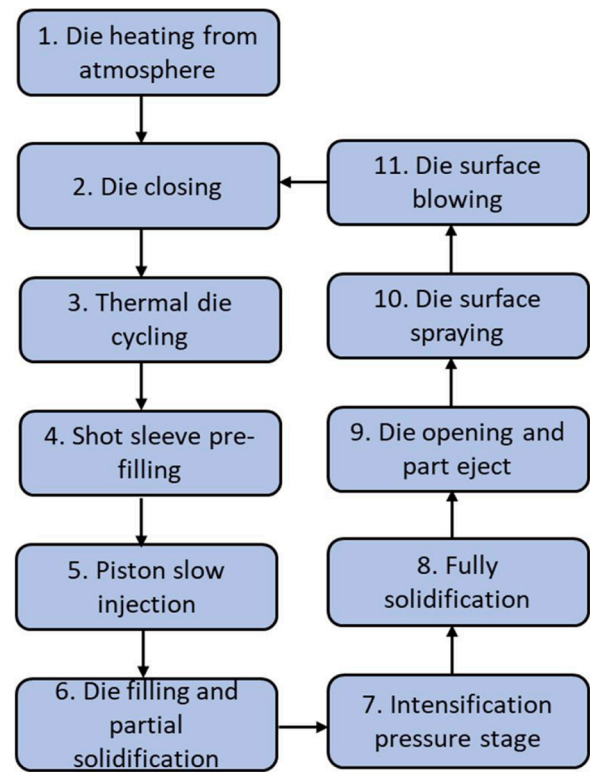


Fig. 2. Typical HPDC procedures during one entire cycle.

plunger velocities in cold chamber HPDC process and found that variation of plunger slow shot/fast shot velocity could affect the distribution of ESCs in final castings and cause the variability in mechanical properties.

Numerical simulation of the HPDC process is not uncommon as researchers and manufacturers are constantly seeking to better understand that which cannot be directly observed during actual practice. Hyuk-Jae [5] studied the design of HPDC gating systems using CAE method and predicted the cast defects accordingly. Gerald [6] studied the optimization of the liquid jet exiting the ingate during HPDC using the smoothed particle hydrodynamics (SPH) method. Cleary [7] studied melt flow characteristics during HPDC and assessed the models accuracy by conducting interrupted filling tests during actual practice. Bruna [8] predicted the re-oxidation process in gating systems for aluminium alloys. Abdel [9] studied the effects of shot sleeve filling on the evolution of the melt free surface and the subsequent solidification process during HPDC using computational fluid dynamics (CFD). It is widely accepted that the poor mechanical properties of HPDC parts, and their highly variable nature, is closely related to the size and spatial distribution of shrinkage/gas porosities, large intermetallic phases and externally solidified crystals that are formed in shot sleeve prior to injection. It follows then, that by developing a better understanding of fluid flow and solidification during HPDC, one may improve product quality and property stability, thus reducing the conservative safety factors commonly used in component design.

Whilst each individual phenomenon influencing the HPDC process has been researched extensively through numerical modelling and experiments, a complete simulation of the HPDC process considering the

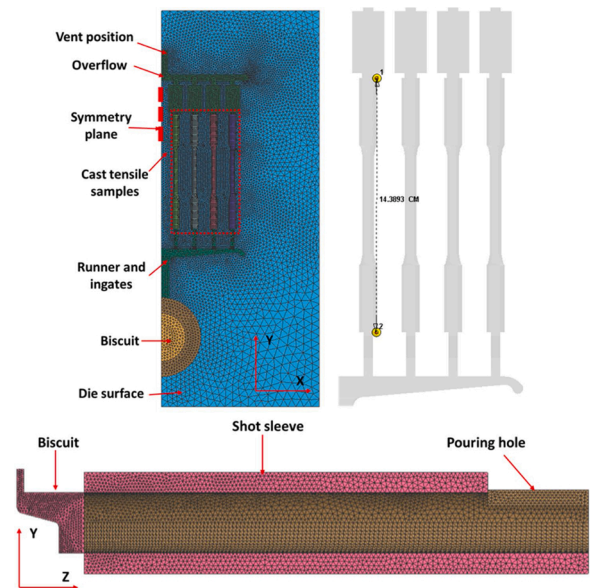


Fig. 3. Configuration and hybrid FEM mesh used in calculation (in 1/2 symmetry) Above: Die and castings dimensions; Below: Shot sleeve and biscuit region.

influence of upstream sub-processes has rarely been seen. That is, to chain the entire HPDC cycle into one mathematical model, which includes die heating, thermal die cycling, shot sleeve pre-filling, slow shot/fast shot injection, die filling/solidification as well as intensification. Once this model is established in its entirety, a series of modelling

Table 1
Initial/boundary conditions used in subsequent modelling.

Alloy type	A356	Shot sleeve temperature	180°C
Liquidus temperature	614°C	Shot sleeve length	480mm
Solidus temperature	553°C	Die and sleeve material	H13 steel
Pouring temperature	680°C	Initial average die surface temperature	150°C
Part ejection time	20s	Die blowing end time	55s

studies could follow, aiming to study the influence of process parameters on melt flow, solidification and defects formation in HPDC and new techniques for suppressing the formation of defects could be obtained, further validated and adopted into industrial practice.

Modelling Procedure and Workflow

In this paper, the entire HPDC process is modelled using the finite element (FEM) method under the ProCAST software platform, which includes three interactive modules: Visual-Mesh, Visual-Cast and Visual-Viewer, which is for FEM mesh generation, model discretization/calculation and result analysis, respectively. The workflow for the modelling process is shown in Fig. 1. During one cycle of the HPDC process, a series of actions are executed in an irreversible order, which can be seen in Fig. 2. In this work, the CAE simulation process is performed following this workflow. The geometrical model of HPDC system is established using CAD software according to real dimensions of the HPDC machine. To save computation time, a symmetrical plane is defined, and half of the model is used for modelling, as can be seen in Fig. 3. After the CAD files are imported and assembled in ProCAST, a hybrid FEM mesh of the entire model is generated. Various mesh sizes are defined according to geometrical features and the desired calculation precision. Initial/boundary conditions of the HPDC process are defined in accordance to actual casting practice, as listed in Table 1. Temperature-dependent material properties of aluminium alloy A356 are calculated using a database provided by the ESI Group, as shown in Fig. 4. Based on this, the entire HPDC process is calculated using the

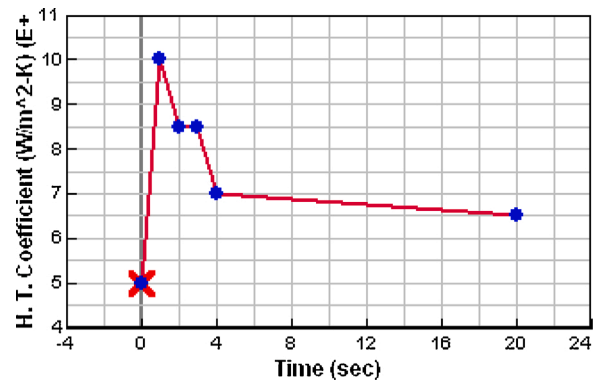


Fig. 5. Time-dependent iHTCs used in this work.

parallel computing technique. The postprocessing module of ProCAST is called to visualize and analyse corresponding modelling results, as illustrated later in this paper.

Model Description

Governing Equations

Melt injection, die filling and solidification of HPDC process are modelled with the ProCAST solver-Visual-Cast. Melt flow, heat transfer and solidification are calculated with 3D finite element method using the following governing equations based on the enthalpy method. Melt turbulence is described using standard k-ε turbulence model. The Volume of Fluid (VOF) method is used to describe the evolution of the melt free surface.

Continuity equation:

$$\frac{\partial \rho}{\partial t} + \nabla \cdot (\rho_i g_i (v)_i) = 0 \tag{1}$$

Momentum equation (simplified):

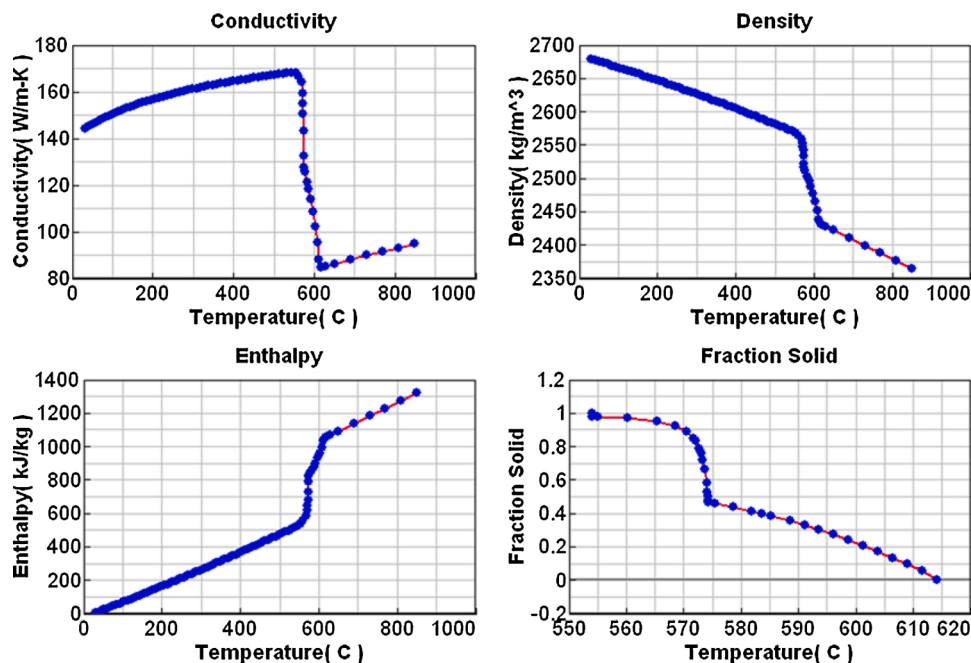


Fig. 4. A356 alloy thermophysical properties.

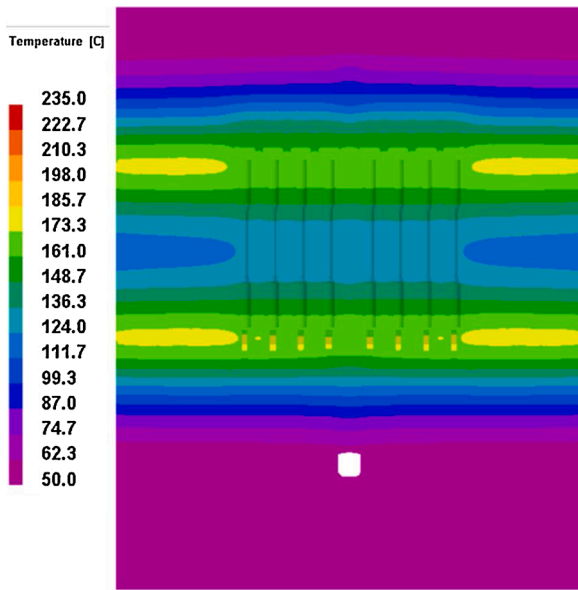


Fig. 6. Temperature distribution on the die surface after heating from atmosphere.

$$\frac{\partial}{\partial t} \left(\frac{\rho_l \langle v_l \rangle}{g_l} \right) + \nabla \cdot \left(\frac{\rho_l \langle v_l \rangle \langle v_l \rangle}{g_l} \right) + \nabla \langle p \rangle_l - \nabla \cdot \left(\frac{\mu_l^{eff}}{g_l} [\nabla \langle v_l \rangle + \nabla \langle v_l \rangle^T] \right) = \rho_l g - \mu_l K^{-1} \langle v_l \rangle \tag{2}$$

Heat flow Equation:

$$\frac{\partial(\rho h)}{\partial t} + \nabla \cdot (\rho_l g_l h \langle v_l \rangle) = \nabla \cdot (k \nabla T) + S \tag{3}$$

Enthalpy constitutive equation:

$$h(T) = \int_0^T C_p(T) dT + L(1 - g_s(T)) \tag{4}$$

In the above equations, $\langle v \rangle_l$ is the intrinsic phase averaged velocity, ρ is the density, p is the pressure, μ_l is the melt viscosity, T is the temperature, C_p is the specific heat, L is the latent heat of solidification, and h is the enthalpy.

Prediction of Trapped Gas and Oxides

In the HPDC process, due to short die filling time and turbulence nature of the melt, the entrainment of air in the final castings are inevitable. In this work, the air entrainment in the final casting is predicted qualitatively combining the ideal gas law and Darcy–Weisbach equation as follows.

$$\frac{\Delta p}{L} = f_D \cdot \frac{\rho \cdot \langle v \rangle^2}{2 \cdot D}$$

Where Δp is the pressure difference for gas before and after die filling, L is the equivalent distance for pressure drop, D is the hydraulic diameter, f_D is the friction coefficient based on wall roughness and D , ρ is related to gas pressure and temperature through ideal gas law. The effect of intensification pressure on the casting is described by defining a critical

Table 2 Thermal die cycling sequence and duration used in modelling.

Sleeve pre-filling duration	3s	Die spraying start time	30s
Piston starts to move	At 3.01s	Die spraying end time	48s
Die opening	At 10s	Die blowing start time	49s
Part ejection time	20s	Die blowing end time	55s

gate solid fraction. If the solid fraction exceeds some critical value (in this case 0.9), the feeding of liquid metal through the ingates is terminated.

For oxide predictions, the oxides indicator within ProCAST software is used, which has the units of (cm²*s). The principle of calculation of this indicator is the following: At each point of the free surface, the free surface area is multiplied by time. This value is cumulated with the value of the previous time step. In addition, this value is transported with the free surface and with the fluid flow. When two free surfaces meet, both values are added. When there is no free surface at a given location, the value of the front tracking indicator will still be transported with the fluid. This indicator allows the user to identify the amount of oxides formed at the free surface and where they are most likely to end up, aiding in the study the flow junctions.

Near-wall flow and heat transfer

For fluid flow near to the wall, flow velocity experiences a boundary layer due to friction between the melt and the shot sleeve and die surfaces. Additionally, impingement of the superheated alloy with the relatively cold shot sleeve or die surface results in time-variant interfacial heat transfer coefficients (iHTCs). In this work, two unique functions WALLF and WSHEAR are established. WALLF is used to compute the velocity of the free surface at the mold wall. The WSHEAR algorithm allows to take into account a velocity boundary layer along mold wall. It allows to have non-zero velocities at the mold walls, which is more representative of the reality (slip of the liquid along walls). Based on filling tests performed by the authors, WALLF and WSHEAR are properly adjusted to describe the fluid flow characteristics near to the wall. Time-dependent iHTCs are then introduced and used in subsequent CAE simulation. Details about previous work can be found in this reference [10]. The evolution of iHTCs is revealed as in Fig. 5.

Simulation Results

Die heating process

Initially, die temperature is assumed to be consistent with that of ambient air (25°C). As the casting process commences, two heating channels in the mobile and stationary platens are switched on to heat the die to working condition. A target temperature of 180°C is set, with the heating channels switching off once this target is achieved. In the model, a dynamic heat boundary condition is applied to heating channel locations and the temperature distribution in the die are calculated accordingly, as depicted in Fig. 6. The calculation results for die heating are further extracted and used as an initial condition for thermal die cycling simulation.

Thermal die cycling process (TDC)

A complete HPDC cycles normally involves several stages including shot sleeve pre-filling, piston slow shot phase, die injection,

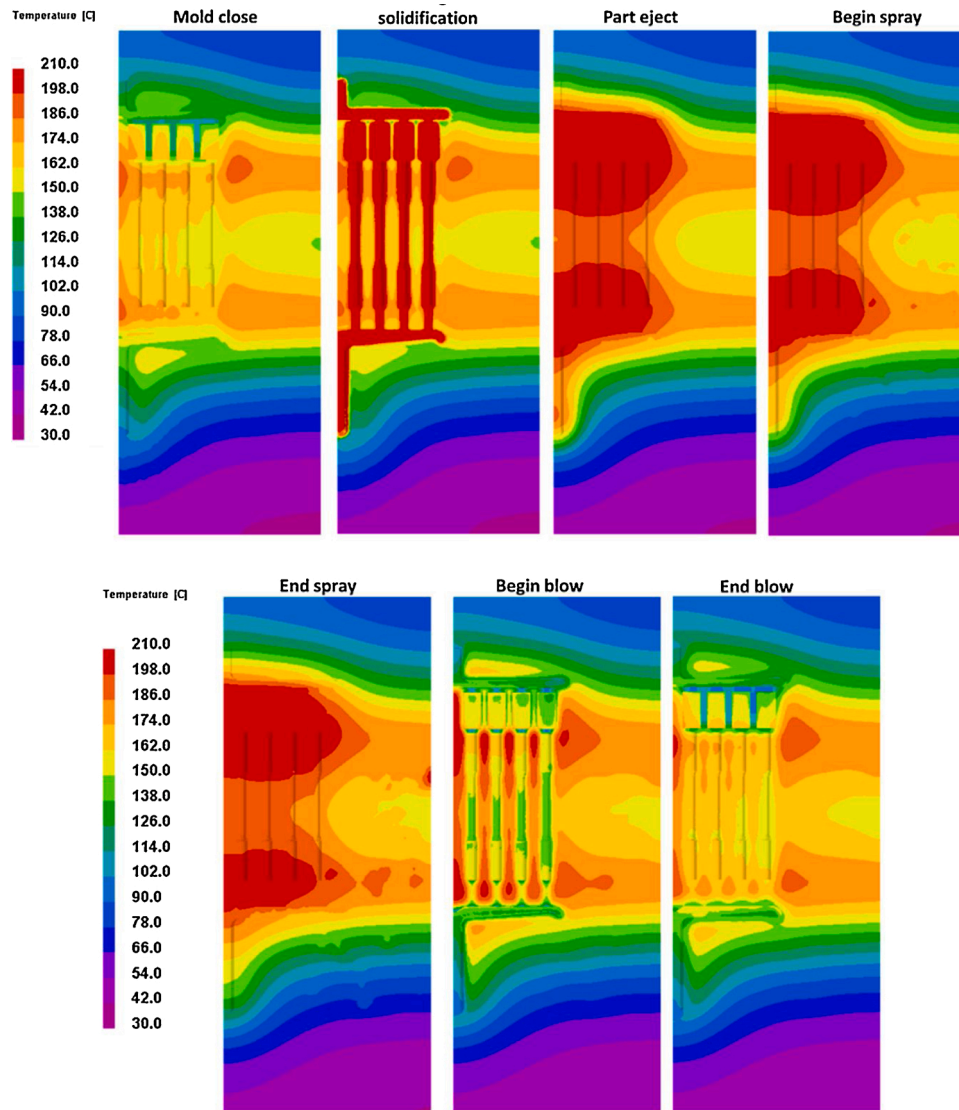


Fig. 7. Temperature distribution at die surface during the 6th HPDC cycle.

intensification, part ejection, die surface spraying and air blowing. In this work, the time durations and sequence of each stages during HPDC are recorded from experiments, as shown in Table 2. Based on the recorded data, a dynamic interfacial heat transfer coefficient function was defined. The thermal die cycling process was calculated for a maximum of 20 cycles. During each stage, the die surface temperature is non-uniform and time-variant. Fig. 7 shows the evolution of temperature on the die surface during the 6th HPDC cycle. It is evident that when the die cavity is filled with liquid metal, the die/melt interface temperature first rapidly increases to some maximum and then stabilizes due to heat transfer. After the solidified casting is ejected from the die cavity, the effect of spraying coolant and blowing air on the die surface temperature is modelled accordingly. This is achieved by defining a spraying/blowing trajectory at die surface as well as spray nozzle shape and its distance from the die. A schematic illustration is shown in Fig. 8.

To further validate the model reliability, a FLIR T6xx series infrared camera was used to capture the die surface temperature during a HPDC cycle operated under the same conditions used in this modelling work. A comparison between the calculated die surface temperature and measured result can be found in Fig. 9, which shows strong agreement regarding the distribution of different temperature ranges. On this basis,

the temperature evolution curves at four locations in the die are plotted during various HPDC cycles, as is depicted in Fig. 10. From this figure, it is clearly observed that after 6~7 cycles, the temperature distribution at the die surface achieves a quasi-steady state. Hence, the temperature distribution on the die surface after 7th HPDC cycle is extracted and mapped for further die filling modelling.

Melt injection and solidification

For the actual HPDC process, a transferring ladle was used to prefill the shot sleeve with melt. In the simulation, this process is modelled with a flowrate-time function (Fig. 11). Fig. 12 shows the sequence of shot sleeve prefill. The left and right figures are colour map of melt temperature from two different angles, respectively. It can be seen that as the melt is poured into the shot sleeve, the temperature of the melt impinging on the sleeve wall drops below the liquidus temperature, resulting in the formation of ESCs along the bottom of the sleeve, as illustrated in Fig. 13.

As the piston continues to move along the shot sleeve, the mixture of molten metal and ESCs is injected into the die cavity. Fig. 14 shows the melt filling sequence in the die cavity. The colour map reveals the air

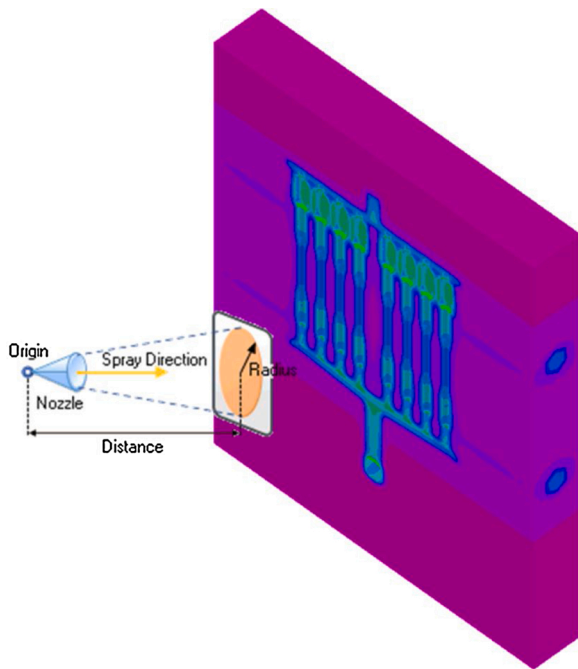


Fig. 8. Schematic illustration of spray/blow after part ejection.

distribution in the casting. It should be noted that the amount of entrained air in the tensile samples at different locations tend to be different owing to varied flow patterns within the die. This phenomenon may prove to be a potential factor influencing the variability of mechanical properties. As the distribution of defects in different locations of castings varies with casting process condition, the existence of defects such as porosity, entrained air, oxides as well as large ESCs would lead to stress concentration in the castings when subject to forces. Therefore, controlling the formation and distribution of solidification defects is key factors in improvement of mechanical properties of HPDC components.

Fig. 15 shows the solidification time of the casting, a cut-off limit of 0.7 s is set and positions where the solidification time is below 0.7 s are visualized. Interestingly, the melt was observed to rapidly solidify at the ingate region shortly after die filling due to the high cooling rate

incurred by the thin ingate thickness (2 mm in this work). Moreover, as is reported by many researchers [11–16], a portion of externally solidified crystals (ESCs) would form in shot sleeve and then be transported into the die cavity through the ingate system. If the ingate regions were to solidify prematurely, the subsequent build-up of ESCs would inhibit the effective transmission of intensification pressure, resulting in poor feeding of the solidifying alloy. To alleviate this problem, it is recommended to keep the ingate region at a relatively high temperature. The proper placement of heating/cooling channels must therefore be carefully considered during the die design stage.

Discussion

In the actual HPDC process, proper configuration of the piston shot curve is beneficial for reducing defects and improving casting efficiency [9,16–19]. A typical shot curve usually comprises of a slow shot stage and a fast shot stage, in which the evolution of piston slow shot velocity along shot sleeve length is important for initial melt free surface development and defects distribution. In this section, the following two aspects are discussed.

Influence of piston slow shot acceleration positions on casting defects distribution

To study the influence of piston slow shot velocity on HPDC defects formation, a series of piston shot curves are selected in which the piston slow shot acceleration position varies as in Fig. 16. In (a)–(d), the piston velocity increases from 0 to 0.2 ms⁻¹ within different distances of 10 mm, 30 mm, 50 mm, and 60 mm from the initial position. After that, the piston slow shot velocity continues to increase to 0.3 ms⁻¹ at the distance of 370 mm along shot sleeve length. In (e), the piston velocity first increases to 0.3 ms⁻¹ and remains constant until reaching the distance of 370 mm. In (f), piston velocity linearly increases from 0 to 0.3 m/s from the initial position to 370 mm. In all of the figures above, the fast shot velocity is kept constant at 3.6 ms⁻¹. Fig. 17 compares the distribution of entrained air in the final casting under the various conditions defined in Fig. 16. It can be seen that due to the complex flow patterns in the die cavity, the amount of entrained air at various locations in the casting differs for each shot condition. The optimum piston slow shot acceleration position is 10 mm from the initial position, in which case the amount and distribution of air in cast tensile samples are less and more uniform according to simulation results. Although the prediction of air entrainment in ProCAST is qualitative, it offers a practical guide for

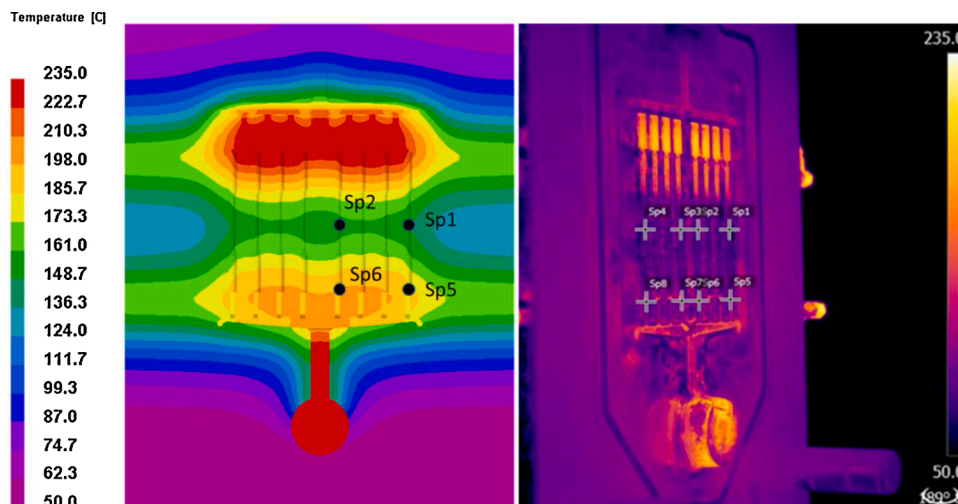


Fig. 9. Comparison of predicted die surface temperature distribution with infrared images obtained during HPDC.

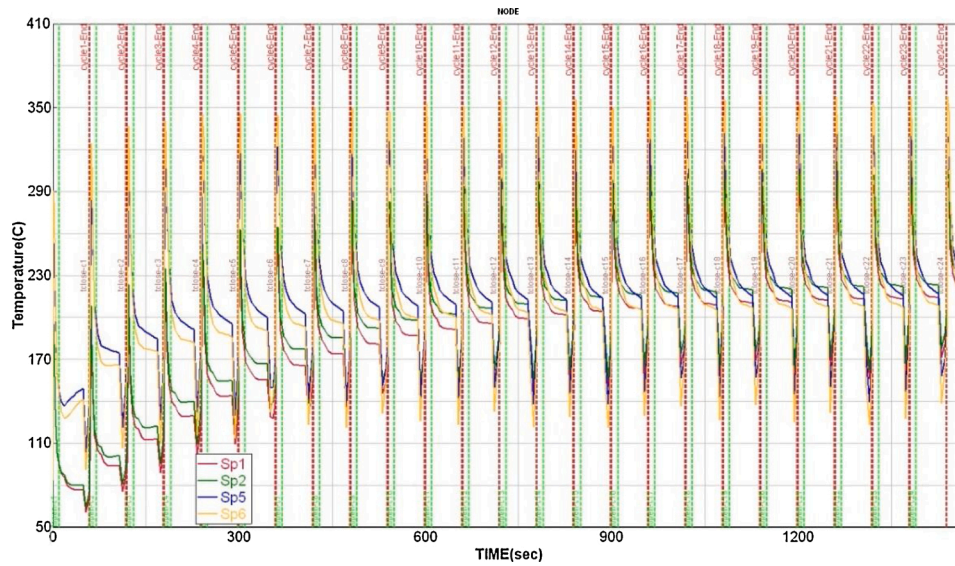


Fig. 10. Calculated temperature curves at sampling positions of die surface at multiple thermal cycles.

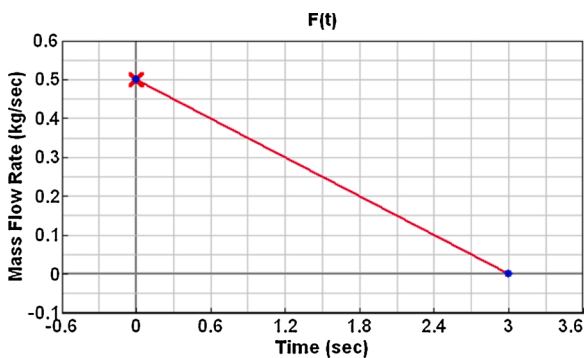


Fig. 11. Flowrate curve used during shot sleeve filling.

determination of piston shot curves and further design considerations and optimization routes for the HPDC process.

Influence of piston slow shot velocity profile on fluid flow and defects formation

To further the influence slow shot velocity on defects formation, three piston shot curves are set as in Fig. 18. The initial piston acceleration position is fixed at 50 mm, while the slow shot velocities for Set 1-1, Set 1-2 and Set 1-3 are 0.2-0.3 ms⁻¹, 0.4-0.6 ms⁻¹ and 0.6-1.0 ms⁻¹, respectively. The modelling results are shown in Fig. 19.

Regarding the melt free surface in the shot sleeve, it is worth noting that the slow shot velocity should not exceed 0.4-0.6 ms⁻¹, otherwise the melt free surface would accumulate and collide with the shot sleeve ceiling too soon, causing further wave collapses and serious air entrainment. Considering the final casting domain, it could be seen that castings produced with a shot slow speed of 0.2-0.3 ms⁻¹ exhibit the lowest level of air entrainment and when the slow shot speed exceeds

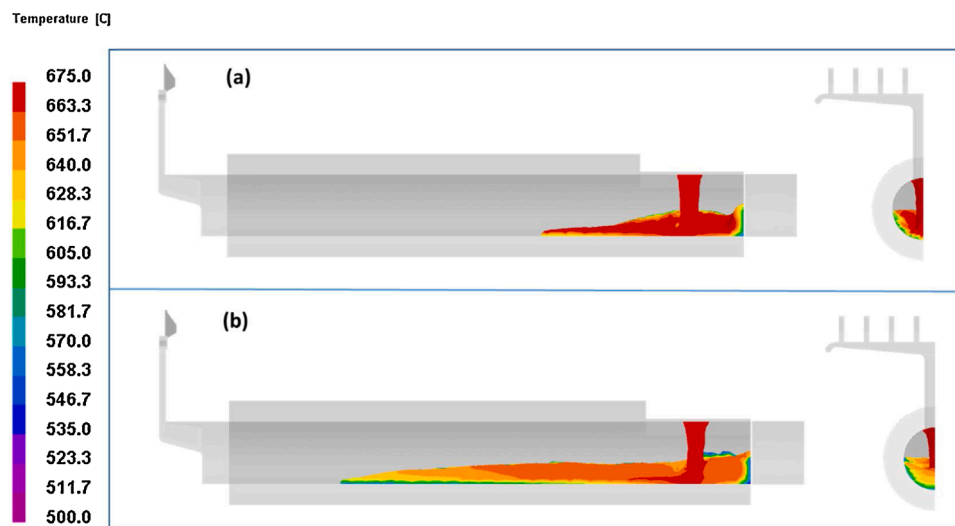


Fig. 12. Flow and temperature evolution of melt during filling of shot sleeve prior to piston injection, images from two viewing angles.

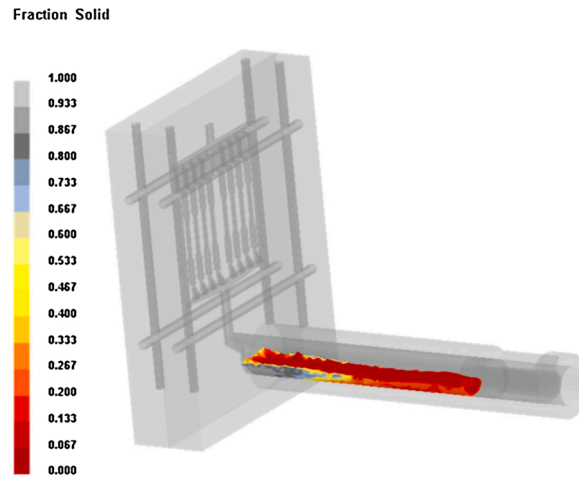


Fig. 13. Distribution of externally solidified crystals along the shot sleeve.

0.6 ms⁻¹, air entrainment in the casting increases and distributes unevenly. Regarding oxide formation and distribution, the optimal slow shot speed is 0.4-0.6 ms⁻¹, under which the oxide tendency at different casting locations are relatively uniform and the amount of oxides tend to be relatively low compared with others condition.

For further comparison, a series of tensile samples are cast using the exact same piston shot curves as mentioned in Fig. 18. The mechanical properties (ultimate tensile strength *UTS*, elongation *El* and yield stress *YS*) of the cast tensile bars are measured and summarized in Table 3. It is seen that *UTS* and *El* values of tensile bars produced using a piston velocity profile of 0.4-0.6 ms⁻¹ exhibit the highest average values and the lowest standard deviations among the three groups.

As the mechanical properties of the casting is a comprehensive result

of casting microstructure and its interaction with defects. Obtaining a uniform microstructure with less defects is the final goal to improve mechanical properties and achieve property stability. For the study in this paper, the increased slow stage velocity of 0.4-0.6 ms⁻¹ could reduce and homogenise oxides formation without introducing excessive air into the melt. It could also limit the formation of externally solidified crystals (ESCs) by reducing heat loss of the melt in shot sleeve.

Conclusion

A complete simulation approach for cold chamber high pressure die casting has been established in ProCAST platform. Based on the FEM, the complete HPDC process including die heating, thermal die cycling, shot

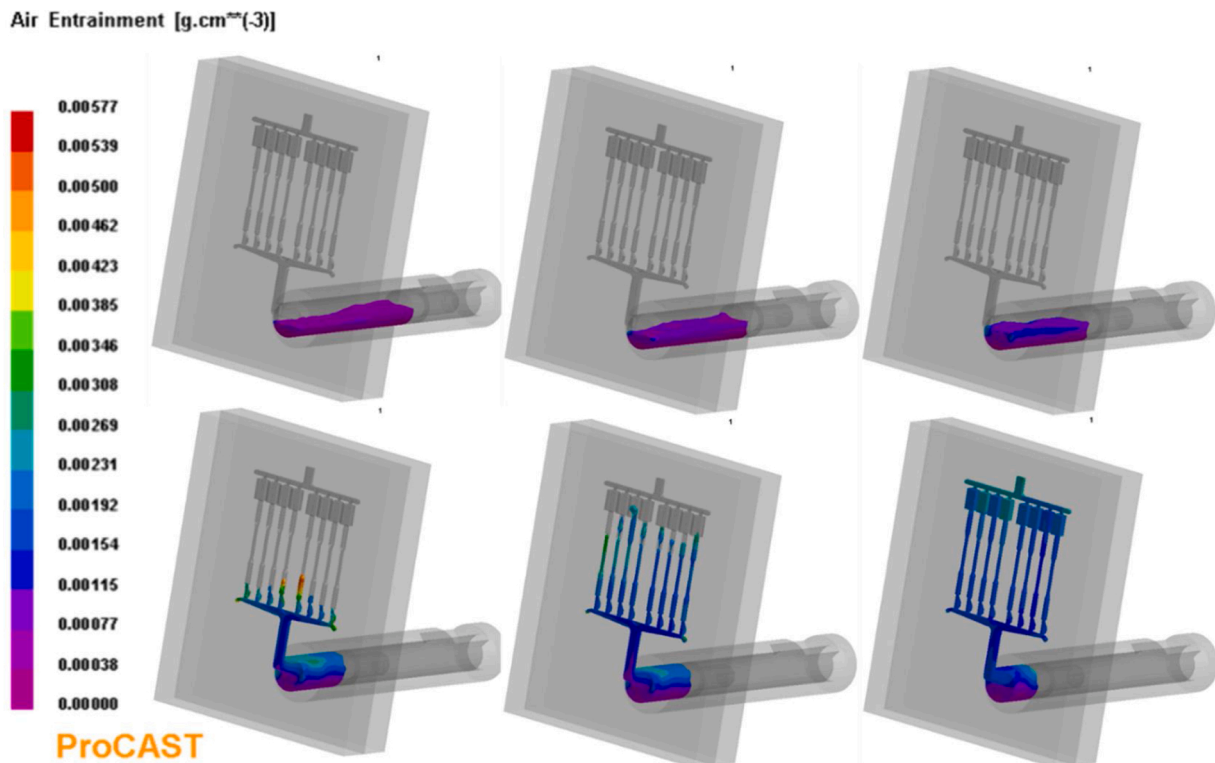


Fig. 14. Filling sequence of the melt and distribution of air in the die cavity.

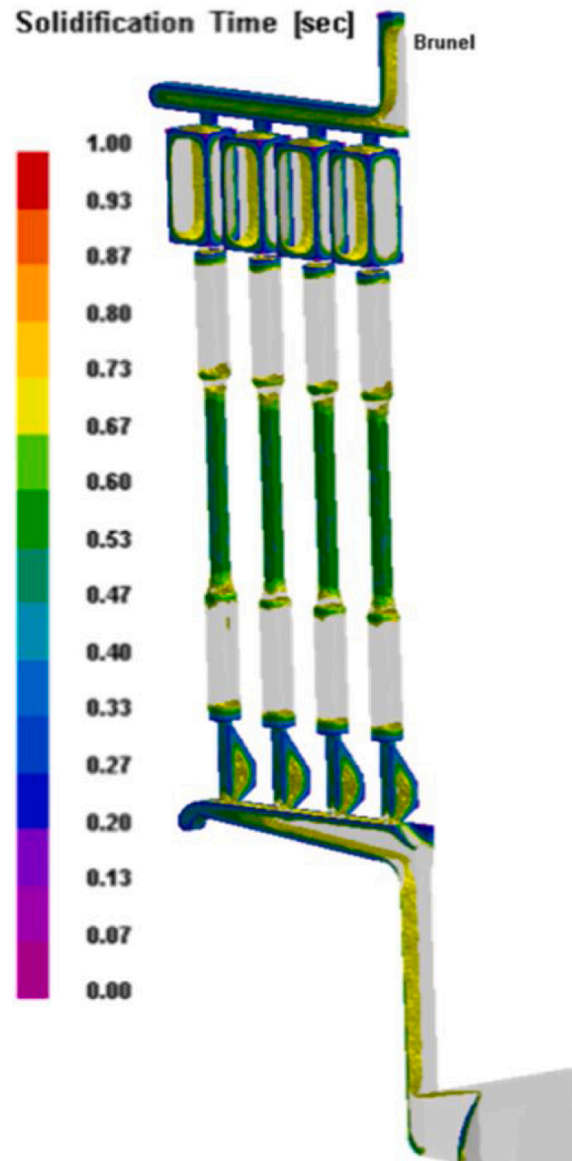


Fig. 15. Section cut-off for position where solidification time is below 0.7 s.

sleeve prefilling, die filling and solidification are modelled and physical phenomena including fluid flow, heat transfer, solidification and defect formation (entrained air, oxides indicator) are studied and visualized with a postprocessing interface. A series of experiments are performed to calibrate the model. Using this entire mathematical model, optimal thermal die cycling is determined to achieve a steady state die temperature. Based on TDC simulation, influence of the piston velocity profile on the formation of defects in tensile bars are studied. Meanwhile, tensile bars produced using the same casting conditions are tested to reveal the link between operational parameters, casting defects and mechanical properties (*UTS*, *YS*, *EI*). Based on the simulation, an optimized piston profile is obtained, which could lead to improved tensile properties in cast tensile samples. The optimum piston slow shot acceleration position is 10 mm from the initial position and the optimal

slow shot speed is $0.4\text{--}0.6\text{ ms}^{-1}$. The complete simulation of HPDC in this work provides CAE engineers with a systematic and cost-effective route to optimizing casting parameters and operating conditions within the HPDC cell, without the need for lengthy empirical trials. In the meantime, the general idea and modelling technique used in this work would contribute to the further development of virtual engineering in metal casting process.

Declaration of Competing Interest

The authors declare that they have no known competing financial interests or personal relationships that could have appeared to influence the work reported in this paper.

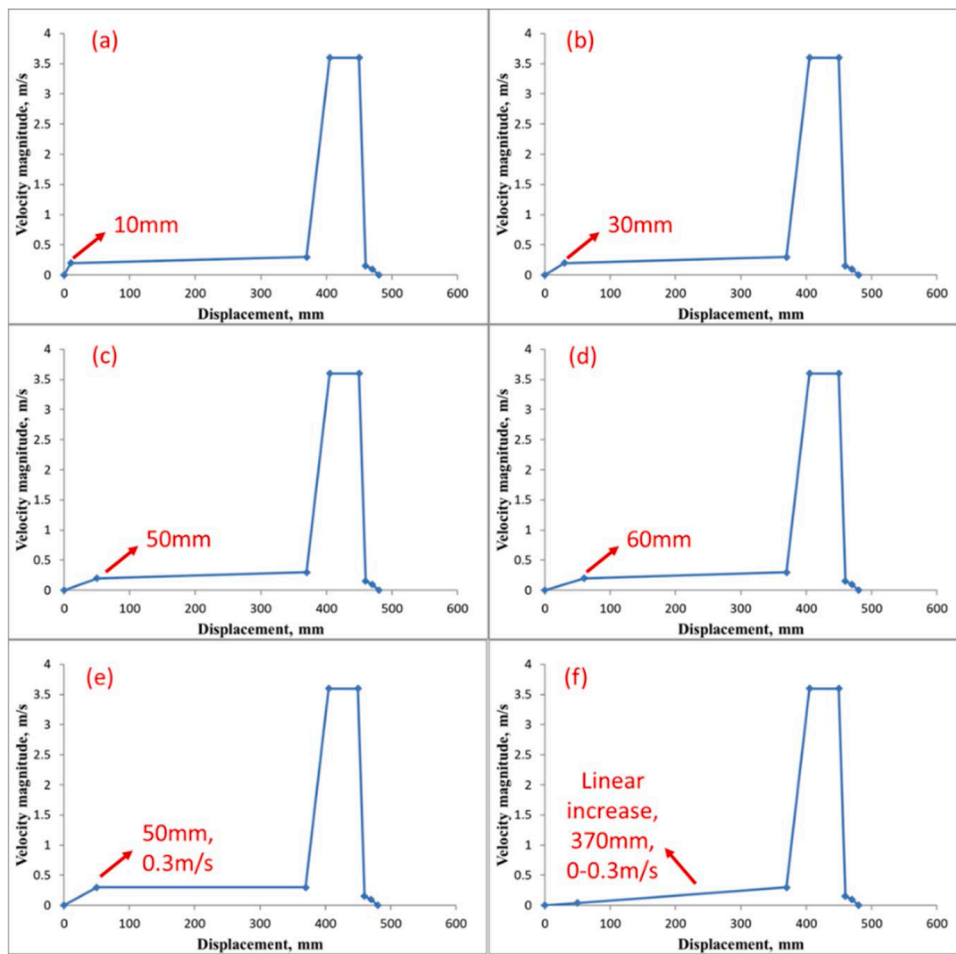


Fig. 16. Piston shot curves with different slow shot acceleration positions.

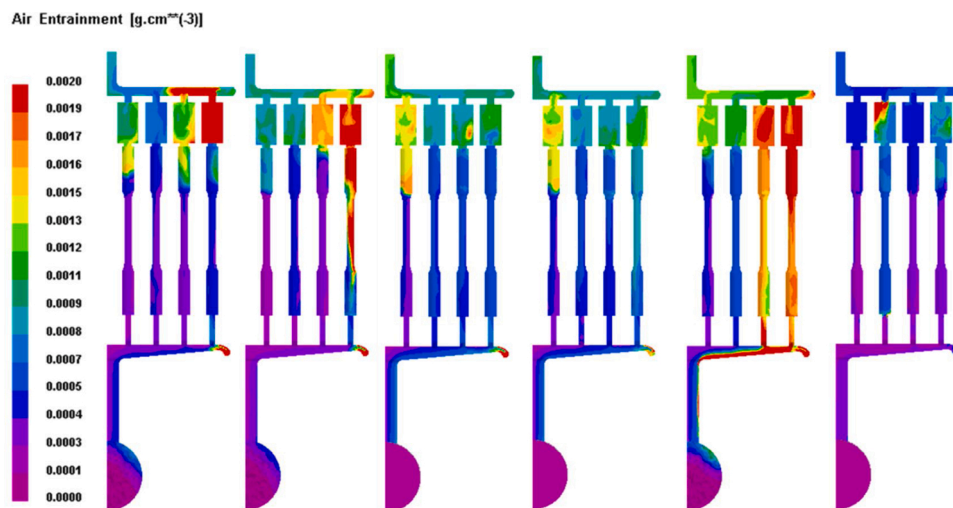


Fig. 17. Modelling results of air entrainment in casting with different slow shot acceleration position (from left to right corresponds to Fig. 13 (a)-(f), respectively).

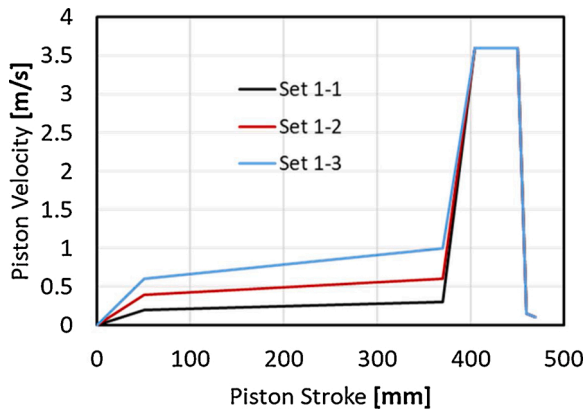


Fig. 18. Piston shot curves with different slow shot velocities.

Table 3

Mechanical properties of tensile samples produced under various piston slow shot profiles.

piston velocity	sample No.	YS (MPa)		UTS (MPa)		El (%)	
			average		average		average
0.2-0.3 m/s	A-1	208.5		348.1		7.6	
	A-2	203.9	206.3	347.0	340.5	6.9	6.0
	A-3	204.6	± 2.0	331.1	± 7.3	4.5	± 1.3
	A-4	208.0		335.6		5.1	
0.4-0.6 m/s	B-1	206.9		348.2		6.1	
	B-2	208.4	204.0	344	344.9	5.6	6.2
	B-3	195.5	± 5.0	344.3	± 1.9	7.4	± 0.7
	B-4	205.3		343.2		5.6	
0.6-1 m/s	C-1	209.7		338.6		5.4	
	C-2	194.5	202.9	343.3	339	6	5.8
	C-3	202.9	± 5.5	339	± 2.9	6.6	± 0.6
	C-4	204.6		335		5.1	

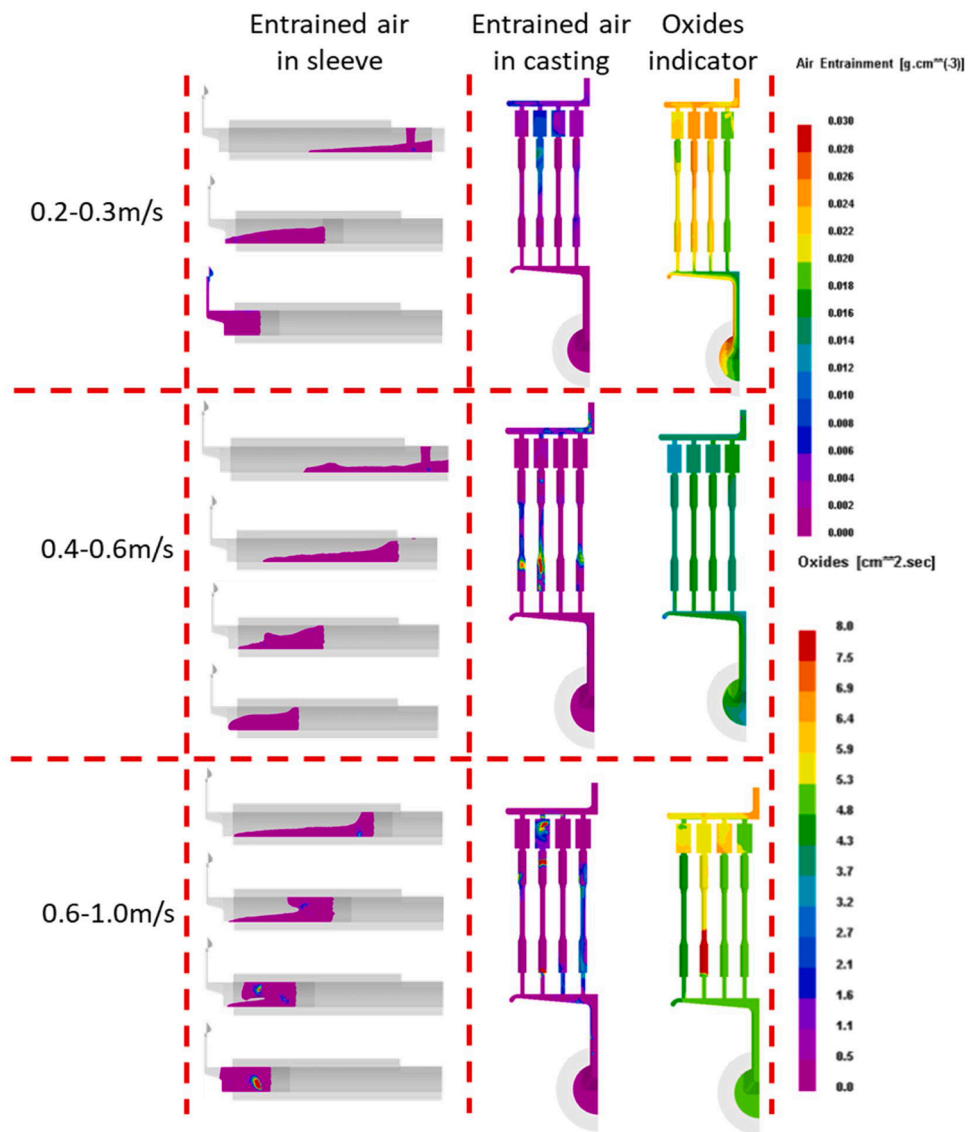


Fig. 19. Comparison of modelling results with different piston slow shot velocity magnitude. First column: evolution of melt free surface and air entrainment in shot sleeve; Second column: air entrainment and oxides indicator in final castings.

Acknowledgements

This project is financially supported by EPSRC UK in the EPSRC Centre for Innovative Manufacturing in Liquid Metal Engineering (The EPSRC Centre—LiME).

References

- [1] Zhou Y, Guo Z, Xiong SM. Effect of runner design on the externally solidified crystals in vacuum die-cast Mg-3.0Nd-0.3Zn-0.6Zr alloy. *J. Mater. Process. Technol.* 2019;267:366–75. <https://doi.org/10.1016/j.jmatprotec.2018.12.032>.
- [2] Gunasegaram DR, Givord M, O'Donnell RG, Finnin BR. Improvements engineered in UTS and elongation of aluminum alloy high pressure die castings through the alteration of runner geometry and plunger velocity. *Mater. Sci. Eng. A.* 2013;559:276–86. <https://doi.org/10.1016/j.msea.2012.08.098>.
- [3] Tsoukalas VD. The effect of die casting machine parameters on porosity of aluminium die castings. *Int. J. Cast Met. Res.* 2003;15:581–8. <https://doi.org/10.1080/13640461.2003.11819544>.
- [4] Wu W, Li X, Guo Z, Xiong S. Effects of process parameters on morphology and distribution of externally solidified crystals in microstructure of magnesium alloy die castings. *China Foundry.* 2018;15:139–44. <https://doi.org/10.1007/s41230-018-7242-z>.
- [5] Kwon HJ, Kwon HK. Computer aided engineering (CAE) simulation for the design optimization of gate system on high pressure die casting (HPDC) process. *Robot. Comput. Integr. Manuf.* 2019;55:147–53. <https://doi.org/10.1016/j.rcim.2018.01.003>.
- [6] Pereira GG, Cleary PW, Serizawa Y. Prediction of fluid flow through and jet formation from a high pressure nozzle using Smoothed Particle Hydrodynamics. *Chem. Eng. Sci.* 2018;178:12–26. <https://doi.org/10.1016/j.ces.2017.12.033>.
- [7] Cleary PW, Ha J, Prakash M, Nguyen T. Short shots and industrial case studies: Understanding fluid flow and solidification in high pressure die casting. *Appl. Math. Model.* 2010. <https://doi.org/10.1016/j.apm.2009.10.015>.
- [8] Brůna M, Bolibruchová D, Pastířák R. Reoxidation Processes Prediction in Gating System by Numerical Simulation for Aluminium Alloys. *Arch. Foundry Eng.* 2017;17:23–6. <https://doi.org/10.1515/afe-2017-0084>.
- [9] Korti AIN, Abboudi S. Effects of shot sleeve filling on evolution of the free surface and solidification in the high-pressure die casting machine. *Int. J. Met.* 2017;11:223–39. <https://doi.org/10.1007/s40962-016-0051-5>.
- [10] Dou K, Lordan E, Zhang YJ, Jacot A, Fan ZY. Numerical simulation of fluid flow, solidification and defects in high pressure die casting (HPDC) process, IOP Conf. Ser. Mater. Sci. Eng. 2019;529:012058. <https://doi.org/10.1088/1757-899X/529/1/012058>.
- [11] Gleeson J, Gourlay CM, Schaffer PL, Laukli HI. Gate microstructure in an AlSi9MgMn High-Pressure Die Casting. *Proc. 12th Int. Conf. Alum. Alloy 2010: 751–6.*
- [12] Cao H, Wessén M. Characteristics of microstructure and banded defects in die cast AM50 magnesium components. *Int. J. Cast Met. Res.* 2005;18:377–84. <https://doi.org/10.1179/136404605225023216>.
- [13] Hong Hai N. Effect of Pressure on Solidification Process and Mechanical Properties During Semi-Solid Casting by Computational Fluid Dynamics (CFD). *Adv. Mater.* 2019;7. <https://doi.org/10.11648/j.am.20180702.15.44>.
- [14] Yuan Z, Guo Z, Xiong SM. Skin layer of A380 aluminium alloy die castings and its blistering during solution treatment. *J. Mater. Sci. Technol.* 2019;35:1906–16. <https://doi.org/10.1016/j.jmst.2019.05.011>.
- [15] Otarawanna S, Gourlay CM, Laukli HI, Dahle AK. Agglomeration and bending of equiaxed crystals during solidification of hypoeutectic Al and Mg alloys. *Acta Mater.* 2010;58:261–71. <https://doi.org/10.1016/j.actamat.2009.09.002>.
- [16] Wang BS, Xiong SM. Effects of shot speed and biscuit thickness on externally solidified crystals of high-pressure die cast AM60B magnesium alloy. *Trans. Nonferrous Met. Soc. China (English Ed.)* 2011;21:767–72. [https://doi.org/10.1016/S1003-6326\(11\)60778-4](https://doi.org/10.1016/S1003-6326(11)60778-4).
- [17] Jiao XY, Wang J, Liu C, Guo Z, Wang J, Wang Z, Gao J, Xiong SM. Influence of slow-shot speed on PSPs and porosity of AlSi 17 Cu 2.5 alloy during high pressure die casting. *J. Mater. Process. Technol.* 2019;268:63–9. <https://doi.org/10.1016/j.jmatprotec.2019.01.008>.
- [18] Yuan L, Xiong S, Liu B, Masayuki M, Yoshihide M, Shingo I. Numerical simulation and optimization of liquid metal flow in the shot sleeve of cold chamber die casting process. *MCWASP Conf. Model. Cast. Welding, Adv. Solidif. Process. Opio, Fr. Miner. Met. Mater. Soc.* 2006:111–8.
- [19] Wang QL, Xiong SM. Effect of multi-step slow shot speed on microstructure of vacuum die cast AZ91D magnesium alloy. *Trans. Nonferrous Met. Soc. China (English Ed.)* 2015;25:375–80. [https://doi.org/10.1016/S1003-6326\(15\)63613-5](https://doi.org/10.1016/S1003-6326(15)63613-5).